

# Preferential CO oxidation in hydrogen (PROX) on ceria-supported catalysts, part I: Oxidation state and surface species on Pt/CeO<sub>2</sub> under reaction conditions

O. Pozdnyakova<sup>a</sup>, D. Teschner<sup>a,b,\*</sup>, A. Wootsch<sup>a</sup>, J. Kröhnert<sup>b</sup>, B. Steinhauer<sup>b</sup>, H. Sauer<sup>b</sup>, L. Toth<sup>c</sup>, F.C. Jentoft<sup>b</sup>, A. Knop-Gericke<sup>b</sup>, Z. Paál<sup>a</sup>, R. Schlögl<sup>b</sup>

<sup>a</sup> Institute of Isotopes, CRC, HAS, POB 77, Budapest, H-1525, Hungary

<sup>b</sup> Department of Inorganic Chemistry, Fritz-Haber-Institut der Max-Planck-Gesellschaft, Faradayweg 4-6, D-14195 Berlin, Germany

<sup>c</sup> Research Institute for Technical Physics and Materials Science, HAS, Budapest, POB 49, H-1525, Hungary

Received 4 September 2005; revised 13 October 2005; accepted 17 October 2005

Available online 17 November 2005

## Abstract

The CO content of hydrogen feed to proton-exchange membrane fuel cells (PEMFCs) must be kept under 1–100 ppm for their proper operation. This can be achieved by using catalysts able to selectively oxidize CO in the presence of excess hydrogen (PROX). The present study reports on the mechanism of the PROX reaction on Pt/CeO<sub>2</sub> catalyst, using catalytic tests, in situ DRIFTS, high-pressure XPS, HRTEM, and TDS techniques. Bulk metallic, pronounced adsorbate-induced surface Pt, and a small amount of oxidized Pt sites were detected by in situ high-pressure XPS under PROX conditions. The preoxidized ceria surface was strongly reduced in pure H<sub>2</sub> but significantly reoxidized under PROX conditions (i.e., O<sub>2</sub> + CO in excess hydrogen) at  $T = 358$  K. The remaining small amount of Ce<sup>3+</sup> decreased with increasing temperature. HRTEM found well-crystallized CeO<sub>2</sub> particles (8–10 nm) in the case of activated (pre-oxidized) sample that transformed in a large extent to an oxygen deficient ceria supercell structure after PROX reaction. Metallic Pt particles (2–3 nm) and small (0.5–0.6 nm) Pt clusters were found by HRTEM. These findings were in accordance with the variations in relative intensity of the corresponding Pt–CO bands (DRIFTS). Different types of carbonate and formate species were detected (XPS and DRIFTS). Their possible role in the reaction mechanism is discussed. Resolved OH bands could not be found by DRIFTS in the PROX reaction mixture indicating significant amount of adsorbed water in a hydrogen-bonded structure. Its presence seems to suppress hydrogen oxidation while CO oxidation still takes place, as the metallic particles are covered by CO (DRIFTS). The direct contribution of surface water in a low-temperature water–gas shift-type reaction in the PROX mixture is proposed.

© 2005 Elsevier Inc. All rights reserved.

**Keywords:** Hydrogen purification; Fuel cell; Preferential CO oxidation; PROX; Platinum; Pt/CeO<sub>2</sub>; Ceria; High pressure XPS; In situ DRIFTS; TDS; HRTEM

## 1. Introduction

Increased attention now turned to development of fuel cell-powered systems, because of their expectedly low environmental impact [1]. The proton-exchange membrane fuel cell (PEMFC) is fueled with clean, CO-free hydrogen, which can be produced by steam reforming (STR), autothermal reforming (ATR), or partial oxidation (POX) of natural gas, light-oil fractions, and alcohols [2,3]. Unfortunately, significant amounts

(ca. 5–15%) of CO are formed together with H<sub>2</sub>, H<sub>2</sub>O, CO<sub>2</sub>, and CH<sub>4</sub>. The concentration of carbon monoxide in the hydrogen feed must be kept below 1–100 ppm for the proper operation of PEMFC [1]. A subsequent water–gas shift (WGS) reaction reduces the amount of CO to 0.5–1% [2]. This amount of CO is still high, and it can be removed by preferential oxidation (PROX) and/or by methanation of CO using mainly Pt and Pt–Ru bimetallic catalysts [4,5].

Several catalytic formulations have been tentatively tested in the PROX reaction so far. Supported noble metals, such as Au [6–9], Pt [6,9–13], Rh [10], Ru [10,14], and the bimetallic Pt–Sn system [12,15], were found applicable for the reaction. In

\* Corresponding author. Fax: +49 30 8413 4676.

E-mail address: [teschner@fhi-berlin.mpg.de](mailto:teschner@fhi-berlin.mpg.de) (D. Teschner).

general, the suitable catalyst must adsorb CO and provide activated oxygen, while hydrogen adsorption must be suppressed. Carbon monoxide is thought to adsorb on the metal phase (Au or Pt). CO adsorption on gold is much weaker than on Pt, however, manifesting itself in low steady-state CO coverage at operational conditions [7–9]. But oxygen does not adsorb on these metals either, because the surface is fully covered by CO (on Pt at  $T < 440$  K [11,13]) or because of the very low sticking coefficient (on Au [16]). Therefore, oxygen should be activated on different sites, either on the reducible support [6–9,13] or—in the case of modified Pt catalysts—on partially oxidized patches, such as Ru(ox) [14], Sn(ox) [15], Ce(ox) [12], or Fe(ox) [17]. In this way, oxygen should diffuse to interface sites and subsequently react either at the perimeter or after a spillover process of one of the components on the adjacent metal/oxide site.

The important role of a reducible support manifests itself in the different behavior of Pt/Al<sub>2</sub>O<sub>3</sub> and Pt on ceria containing supports in the PROX reaction [13]. Supporting Pt on Al<sub>2</sub>O<sub>3</sub> results in increasing O<sub>2</sub> conversion and a maximum CO conversion as a function of temperature at around 440 K in the PROX reaction [10,11,13], whereas oxygen conversion on Pt/CeO<sub>2</sub> is very high even at low temperature, with a sharp “light off” activity at around 363 K [13]. The maximum selectivity as a function of temperature was observed at much lower temperature on Pt/CeO<sub>2</sub> than on Pt/Al<sub>2</sub>O<sub>3</sub>, and, accordingly, the maximum CO conversion appears at a temperature of around 370 K on the former sample [13]. The different behavior of the samples is interpreted by different reaction mechanisms [13]. On Pt/Al<sub>2</sub>O<sub>3</sub>, a competitive Langmuir–Hinshelwood kinetics can be supposed, because Pt can adsorb all reactants involved. On ceria-supported Pt, a noncompetitive Langmuir–Hinshelwood mechanism has been described, involving CO activation on Pt particles and their reaction with oxygen activated from the support on the metal/oxide interface at low temperature ( $T = 363$ – $423$  K). Both competitive and noncompetitive reaction pathways, as well as reaction on the ceria support, have been proposed for higher temperatures [13].

From a more general standpoint, cerium oxide is active in transient oxygen storage, and as a catalyst support, it can promote oxidation even under oxygen-poor conditions [18]. Ceria-supported platinum [19,20], rhodium [21,22], and palladium [23] catalysts are also remarkably active in the low-temperature oxidation of CO, and they are able to oxidize carbon monoxide even in the absence of oxygen, in the so-called “oxygen storage capacity” (OSC) measurement [24–26].

A number of studies have been devoted to ceria-containing catalysts, investigating chemisorptive [27,28], structural [29,30], and catalytic properties [18,31]. Adsorption of CO on ceria-supported catalysts leads to the accumulation of various carboxylate, carbonate, and formate species on the ceria surface, as shown on infrared spectroscopic studies [32–37]. The oxidation state of ceria was also studied after different pretreatments by XPS [38–40]; it was found that hydrogen exposure leads to a high concentration of Ce<sup>3+</sup> at surface and subsurface sites, and also that the surface layer of partly reduced ceria easily reoxidizes after exposure to O<sub>2</sub> at room temperature.

Various direct and indirect experimental evidence has been presented for the reaction mechanism in the PROX reaction on ceria-supported Pt [13]; nevertheless, some controversy and yet-unresolved questions remain. For example, what is the surface state of the catalysts during the reaction? Is Pt reduced in the presence of the PROX mixture despite the oxidizing preconditioning? Is the reduction degree of reducible oxides crucial to supply activated oxygen to the reaction? Can the strong temperature dependence of the selectivity on Pt/CeO<sub>x</sub> also be explained simply by changes in the CO coverage, as has been suggested for alloy samples [14,15]? What are the possible surface species formed during the PROX reaction? Are they the same species as formed during CO oxidation (without hydrogen)?

To gain further insight into the reaction mechanism of the PROX reaction on Pt/CeO<sub>2</sub> catalysts, we examined changes in the oxidation state of ceria and Pt occurring under various reaction environments by high-pressure XPS, as well as the surface species formed after adsorption of CO alone, CO + O<sub>2</sub>, or CO + H<sub>2</sub> + O<sub>2</sub> (PROX mixture) onto oxidized catalysts by in situ DRIFTS. In a companion paper (Part II), we report on Pd/CeO<sub>2</sub> catalysts using the same techniques; because the palladium samples are far less active in the PROX reaction, we compare the two systems to obtain a better understanding of the reaction mechanism.

## 2. Experimental

### 2.1. Catalysts

Two catalysts with nominally 1 and 5% metal loadings were prepared on ceria support (Rhodia Catalysts & Electronics, France; BET = 96 m<sup>2</sup> g<sup>-1</sup> [41]) by wet impregnation with an aqueous solution of Pt(NH<sub>3</sub>)<sub>4</sub>(OH)<sub>2</sub> [13,42]. The impregnated samples were dried at 393 K overnight and calcined for 4 h at 773 K in flowing air (30 mL/min), then reduced at 673 K for 4 h in flowing H<sub>2</sub> (30 mL/min). Dispersion was determined by low-temperature (223 K) H<sub>2</sub> adsorption after reduction [43,44]. The obtained values were  $D = 62\%$  for 1% Pt/CeO<sub>2</sub> and 18% for 5% Pt/CeO<sub>2</sub>.

### 2.2. Catalysis

Catalytic tests were carried out in an atmospheric continuous-flow glass reactor system with stainless steel tubing and connections. Analytical-grade hydrogen, oxygen, and CO were used as inlet gases and controlled by Brooks mass-flow controllers calibrated earlier. Product analysis was performed by a gas chromatograph (TCD) equipped with a polar column (Poropak Q) to separate CO<sub>2</sub> and H<sub>2</sub>O from the other effluent gases, as well as by a hydrogen compensated flue-gas analyzer (MRU DELTA 65-3) for CO and O<sub>2</sub> quantification. Only CO<sub>2</sub> and H<sub>2</sub>O were detected as products; methane did not appear in our experimental conditions. The total gas inlet was 100 N mL/min, containing 1% CO, 0.4–1% O<sub>2</sub> (oxygen excess,  $\lambda$ , 0.8–2), and the rest H<sub>2</sub>.

Catalysts were activated in situ in flowing air (30 mL/min) at 573 K before catalytic testing. A charge of 82 mg 1% Pt/CeO<sub>2</sub> and 73 mg 5% Pt/CeO<sub>2</sub> was used in the catalytic reactor and reactivated between different measurement series by the aforementioned treatment [13]. CO and O<sub>2</sub> conversion, as well as the selectivity, were calculated as reported previously [13].

The *total conversion* was defined as the oxygen consumption,

$$X_{\text{total}} = X_{\text{O}_2} = \frac{n_{\text{O}_2}^{\text{in}} - n_{\text{O}_2}^{\text{out}}}{n_{\text{O}_2}^{\text{in}}} \times 100 (\%). \quad (1)$$

CO conversion, considering no side-reactions, can be defined as

$$X_{\text{CO}} = \frac{n_{\text{CO}}^{\text{in}} - n_{\text{CO}}^{\text{out}}}{n_{\text{CO}}^{\text{in}}} \times 100 = \frac{n_{\text{CO}_2}^{\text{out}}}{n_{\text{CO}}^{\text{in}}} \times 100 (\%). \quad (2)$$

*Selectivity* is defined as the ratio of the oxygen transformed into CO<sub>2</sub> to the total oxygen consumed as

$$S = \frac{n_{\text{CO}_2}^{\text{out}}}{2(n_{\text{O}_2}^{\text{in}} - n_{\text{O}_2}^{\text{out}})} \times 100 (\%). \quad (3)$$

The relation between conversion and selectivity is defined as

$$X_{\text{CO}} = \frac{SX_{\text{O}_2}}{100} \lambda (\%), \quad (4)$$

where  $\lambda$  is the oxygen excess factor, by definition,

$$\lambda = \frac{2n_{\text{O}_2}^{\text{in}}}{n_{\text{CO}}^{\text{in}}} = \frac{2p_{\text{O}_2}}{p_{\text{CO}}} = \frac{2[\text{O}_2]^{\text{in}}}{[\text{CO}]^{\text{in}}} = \frac{2c_{\text{O}_2}^{\text{in}}}{c_{\text{CO}}^{\text{in}}}. \quad (5)$$

### 2.3. Temperature-programmed desorption

Temperature-programmed desorption (TDS) measurements were performed in a standard UHV apparatus equipped with an atmospheric chamber. The atmospheric part was used to introduce the sample for pretreatments and adsorbing gases at non-UHV pressures. The 5% Pt/CeO<sub>2</sub> was investigated by TDS. Different gases (gas mixtures) were adsorbed at room temperature on the sample: CO alone (10<sup>-2</sup> mbar for 30 min), CO + O<sub>2</sub> (10<sup>-2</sup> mbar O<sub>2</sub> + 2 × 10<sup>-2</sup> mbar CO for 20 min), and H<sub>2</sub> + CO + O<sub>2</sub> (4.7 × 10<sup>-1</sup> mbar H<sub>2</sub> + 2 × 10<sup>-2</sup> mbar CO + 10<sup>-2</sup> mbar O<sub>2</sub> for 20 min). After adsorption, the sample was evacuated and transferred to the UHV chamber to follow the desorption pattern. The heating rate was 1 K/s. A Balzers mass spectrometer was used to follow the evolution of desorbing gases.

### 2.4. In situ diffuse reflectance infrared spectroscopy

A diffuse reflection attachment “Selector” from Graseby Specac was placed in a Bruker FTIR spectrometer equipped with a D315M MCT detector to collect diffuse reflectance infrared (DRIFT) spectra. The spectrometer was purged with purified air. Reactions were conducted in a gold cup (2.5 mm high, 8.5 mm o.d., 7.2 mm i.d.) placed in a Graseby Specac “environmental chamber” with a ZnSe window. A spectrum of KBr recorded in N<sub>2</sub> served as background. Inlet gases were analyti-

cal grade and controlled by mass flow controllers. The total gas inlet was 50 N mL/min, containing 1% CO in N<sub>2</sub> (referred to as CO alone), 1% CO and 1% O<sub>2</sub> in N<sub>2</sub> (CO + O<sub>2</sub>), or 1% CO and 1% O<sub>2</sub> in H<sub>2</sub> (PROX).

All measurement series were carried out on ca. 100 mg of fresh sample previously pretreated in situ in flowing air (30 mL/min) at 573 K. The catalyst was purged in N<sub>2</sub> while cooling to the desired reaction temperature of 383 or 523 K. A spectrum of the activated sample before adsorption was collected in N<sub>2</sub> at the reaction temperature, and then the reaction mixture—premixed in a bypass—was introduced to the catalyst in one step. Spectra were collected as a function of time on stream for 90 min in all cases. Only spectra taken under the steady-state conditions are shown herein.

Gas composition was analyzed only in the case of PROX reaction by a Pfeiffer Thermostar mass spectrometer. Selectivity and activity values were calculated using the same formula as presented earlier.

### 2.5. High-pressure X-ray photoelectron spectroscopy

The in situ XPS experiments were performed at beamline U49/2-PGM2 at BESSY in Berlin. Details about the setup were published [45–47]. Briefly, the differentially pumped electrostatic lens system is the key feature of the system, allowing investigation of the sample in the mbar pressure region.

The 5% Pt/CeO<sub>2</sub> sample was chosen for these measurements to ensure a reliable signal-to-noise ratio in the Pt 4f region. A pressed pellet containing about 100 mg of 5% Pt/CeO<sub>2</sub> catalyst was placed on a temperature-controlled heater, and was then activated in situ in oxygen (0.5 mbar, 573 K). Gas flow (~20 N mL/min) into the reaction cell was controlled using calibrated mass flow controllers and leak valves. The PROX mixture contained 0.48 mbar H<sub>2</sub>, 0.032 mbar CO, and 0.015 mbar O<sub>2</sub>. Gas-phase analysis was carried out using a quadrupole Balzers mass spectrometer connected through a leak valve to the experimental cell. Selectivity and activity values were calculated using the same formulas as presented earlier.

Ce 3d, O 1s, C 1s, and Pt 4f spectra were recorded with photon energies of  $h\nu = 1035, 650$  (and 920), 670, and 460 eV, respectively. The binding energies (BEs) were calibrated, if possible, against the Fermi level of the sample or using internal references, such as the Ce 3d V (882.4 eV) and U''' (916.7 eV) hybridization states [48] or the Ce 4f state in the band gap. The energy calibration was necessary because surface charging occurred due to the emission of photoelectrons. In the presence of hydrogen (i.e., in most cases) this was only 1–3 eV, in O<sub>2</sub>, however, charging up to 20 eV was observed. Decomposition of the Pt 4f and C 1s regions was performed using Gauss–Lorentz curves. The metallic Pt 4f component at 71 eV was fitted using Gauss–Lorentz profiles with an exponential tail.

### 2.6. High-resolution transmission electron microscopy

High-resolution transmission electron microscopy (HRTEM) investigations were performed in a Philips CM200 FEG elec-

tron microscope operated at 200 keV. The microscope was equipped with a Gatan imaging filter (GIF 100), Gatan Slow-Scan Camera, and EDX system. The sample was prepared from a piece of the 5% Pt/CeO<sub>2</sub> pellet that was previously activated in O<sub>2</sub> in the in situ XPS cell as was done for the in situ XPS experiments. Another sample of 5% Pt/CeO<sub>2</sub> was also investigated after PROX reaction at 358 K (from the XPS cell).

### 3. Results

#### 3.1. Catalytic reaction

Fig. 1 compares the CO oxidation activity on 1% Pt/CeO<sub>2</sub> in the absence and presence of hydrogen. A sharp “light off” activity around 365 K was observed at high oxygen excess without hydrogen, which became less pronounced with decreasing oxygen excess (Fig. 1a), in accord with earlier observations [19–21]. In the presence of hydrogen, the oxygen conversion (not shown) was very high (ca. 98–100%), whereas CO conversion decreased as a function of temperature [13]. The oxygen was consumed for the production of water. Nevertheless, the natural selectivity of Pt toward CO oxidation as opposed to H<sub>2</sub> oxidation, manifested as lower  $\lambda$  values, resulted in higher selectivity (Fig. 1c).

The catalytic data observed in different experimental setups are compared in Table 1. Unfortunately, the 1% Pt/CeO<sub>2</sub> sample could not be measured by XPS because of the low Pt content. To receive well-resolved Pt spectra in the high-pressure XPS apparatus, the 5% Pt/CeO<sub>2</sub> sample was prepared and measured here.

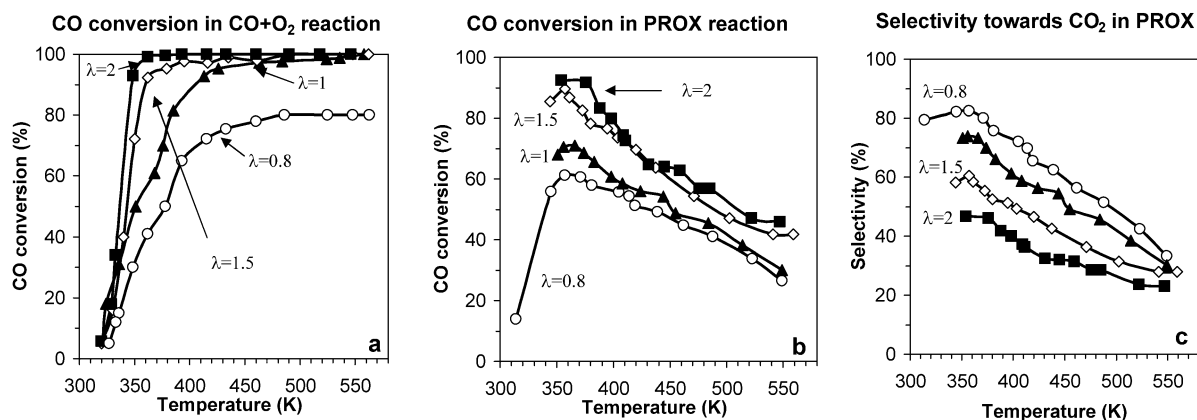


Fig. 1. CO oxidation activity in the absence (a) and presence of hydrogen, PROX (b) as well as selectivity towards CO oxidation in the PROX reaction (c) on 1% Pt/CeO<sub>2</sub> catalyst as a function of temperature at different oxygen excess  $\lambda$ . The oxygen conversion was almost total in the PROX reaction under all conditions.

Table 1  
PROX reaction in different experimental setups and on different catalysts. Reaction mixtures contained 1% CO, 0.5 or 1% O<sub>2</sub> (O<sub>2</sub> excess  $\lambda = 1$  or 2) in H<sub>2</sub>. Total pressure:  $p = 1$  atm in catalytic reactor and DRIFTS cell and  $p = 0.5$  mbar in high pressure XPS

	Catalytic reactor								DRIFTS		XPS	
	1% Pt/CeO <sub>2</sub>				5% Pt/CeO <sub>2</sub>				1% Pt/CeO <sub>2</sub>		5% Pt/CeO <sub>2</sub>	
O <sub>2</sub> excess ( $\lambda$ )	1	1	2	2	1	1	2	2	2	2	1	1
T (K)	383	523	383	523	383	523	383	523	383	523	358	523
X <sub>CO</sub> (%)	65	38	83	47	59	41	84	42	44	22	9	6
S (%)	66	38	42	24	60	41	43	21	30	14	83	18
X <sub>O<sub>2</sub></sub> (%)	99	100	99	100	98	100	99	100	73	81	12	38

DRIFTS results are shown mainly on the 1% Pt/CeO<sub>2</sub>. Both catalysts were tested in the catalytic reactor, and 1% Pt showed slightly better performance in the PROX reaction; however, this difference was negligible (Table 1).

Activity patterns measured in different setups showed similar trends, albeit with different actual values (Table 1). In all cases, increasing temperature decreased the selectivity toward CO oxidation, and the lower O<sub>2</sub> conversion was, as a rule, accompanied by higher selectivity toward CO oxidation. The differences in activity pattern can be attributed to the different contact times due to the varying dead volume and volume flow rates in the different experimental setups. In the flow reactor system, the sample covers the whole cross-section of the reactor, whereas in the DRIFTS experiments, the gas mixture passes over the catalyst powder in a ca. 100-cm<sup>3</sup> cell. In the case of high-pressure XPS, the 10-mm-diameter pellet was placed in a ca. 8-L chamber, and the total pressure was only 0.5 mbar, as opposed to the atmospheric pressure used in other setups.

#### 3.2. Temperature-programmed desorption (TDS)

Fig. 2 shows the desorption curves of CO<sub>2</sub> and water from the 5% loading catalyst after adsorbing different gases or gas mixtures. Formation of CO<sub>2</sub> after adsorption of CO alone clearly occurred, but its amount was an order of magnitude lower than the amount desorbed after oxygen-containing mixtures. Interestingly, more CO<sub>2</sub> was produced in the presence of hydrogen, particularly around 358 K. Water desorption was very strongly enhanced after adsorption of PROX mixture espe-

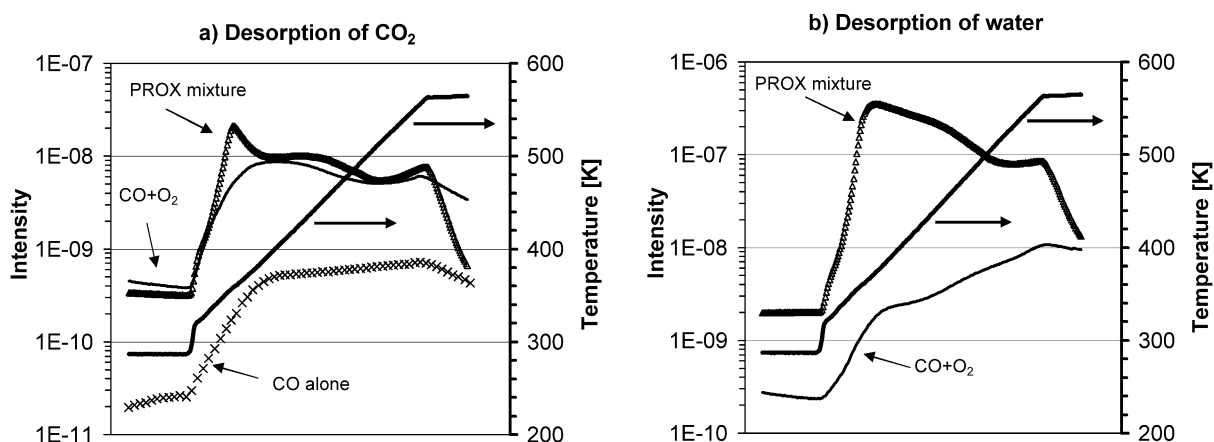


Fig. 2. Temperature-programmed desorption (TDS) curves of CO<sub>2</sub> (a) and water (b) from the 5% loading catalyst after adsorbing different gas mixtures at room temperature: CO alone corresponds to 10<sup>-2</sup> mbar CO for 30 min, CO + O<sub>2</sub> to 10<sup>-2</sup> mbar O<sub>2</sub> + 2 × 10<sup>-2</sup> mbar CO for 20 min, and PROX mixture 4.7 × 10<sup>-1</sup> mbar H<sub>2</sub> + 2 × 10<sup>-2</sup> mbar CO + 10<sup>-2</sup> mbar O<sub>2</sub> for 20 min. (Intensities are shown as measured, without calibration.)

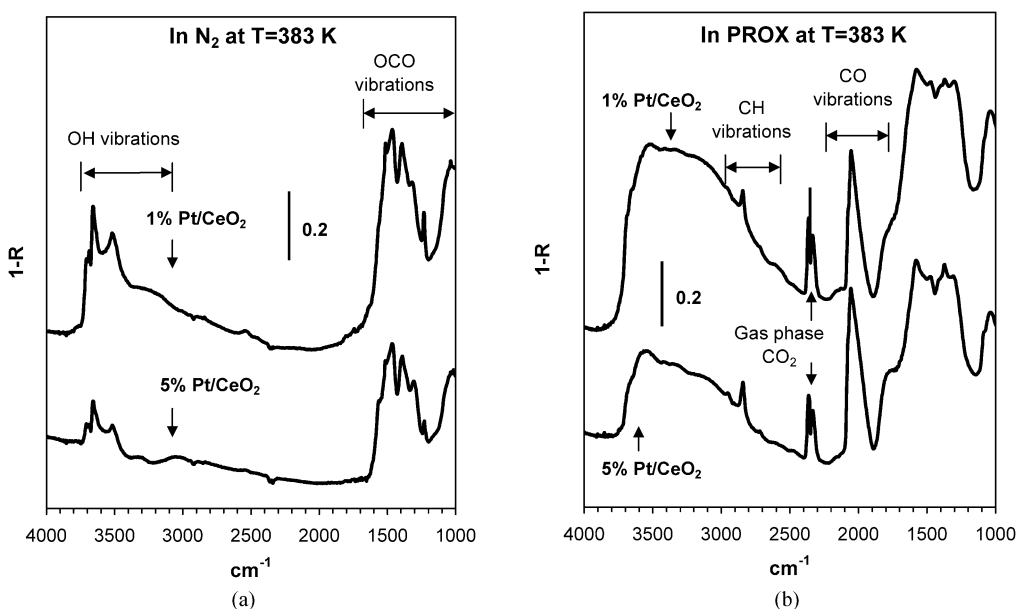


Fig. 3. DRIFT spectra of 1 and 5% Pt/CeO<sub>2</sub> at  $T = 383$  K (a) after activation in N<sub>2</sub> and (b) in the presence of PROX reaction mixture (1% CO, 1% O<sub>2</sub> in H<sub>2</sub>).

cially up to 500 K. Its amount (after calibration) was an order of magnitude higher than expected considering the selectivity values given in Table 1.

### 3.3. In situ DRIFTS

DRIFT spectra of 1 and 5% Pt/CeO<sub>2</sub> samples recorded after activation in oxygen as well as in different reaction environments (CO alone, CO + O<sub>2</sub>, and PROX mixture) exhibited similar features irrespective of the metal loading (Fig. 3). Therefore, the discussion from now on is limited to the 1% Pt/CeO<sub>2</sub> sample. For clarity, the spectral features observed for four characteristic vibrational regions are presented separately (Figs. 4–7), and the characteristic bands corresponding to different surface species are summarized in Tables 2–4.

#### 3.3.1. DRIFT spectra in the region 2200–1700 cm<sup>-1</sup>

The DRIFT spectra of CO adsorbed on the 1% Pt/CeO<sub>2</sub> under different conditions in the region of 2200–1700 cm<sup>-1</sup> are

shown in Fig. 4. The bands in this region are summarized in Table 2. Adsorption of CO on Pt/CeO<sub>2</sub> at 383 K in the absence of both oxygen and hydrogen produced one main band at 2063 cm<sup>-1</sup>, with significant broadening at the low-frequency side, and shoulders at about 2095 and 2083 cm<sup>-1</sup> (Fig. 4a). The strong band at 2063 cm<sup>-1</sup> and the shoulder at about 2083 cm<sup>-1</sup> could be attributed to linear CO species adsorbed on a step-site and terrace Pt<sup>0</sup> atoms, respectively (Table 2) [15,32,34,35]. The shoulder at ~2095 cm<sup>-1</sup> is due to CO adsorbed on a partly oxidized Pt site in the vicinity of reduced Pt [32,34,35]. The broad band at ca. 1970–1960 cm<sup>-1</sup> recalls the feature observed at 2000–1960 cm<sup>-1</sup> on Pt/Al<sub>2</sub>O<sub>3</sub> and Pt/CeO<sub>2</sub>-SiO<sub>2</sub> catalysts and is assigned to CO adsorption at the metal-support interface [49–52]. Kappers et al. [53] attributed this downshift of the  $\nu(\text{CO})$  band as an indicator of ion-dipole interaction between O atom of the CO species with charged cations from the support. They showed that adsorbed water can preferentially shield this interaction. A weak  $\nu(\text{CO})$  band characteristic of bridge-

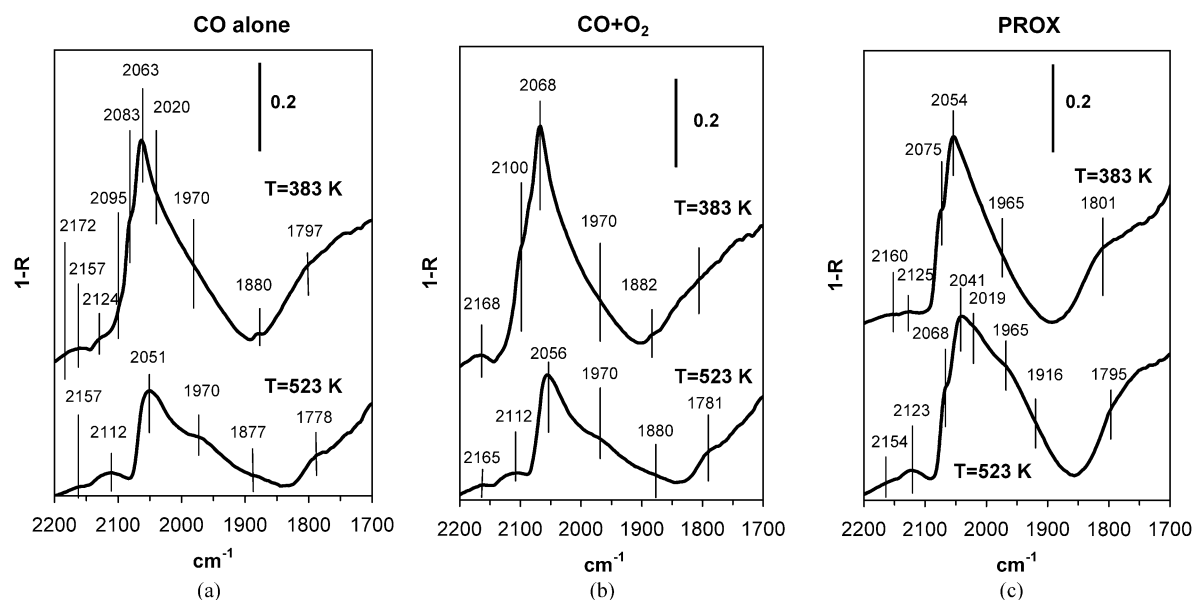


Fig. 4. DRIFT spectra in the 2200–1700  $\text{cm}^{-1}$  region (CO vibrations) of 1% Pt/CeO<sub>2</sub> in the presence of (a) 1% CO alone in N<sub>2</sub>, (b) in 1% CO and 1% O<sub>2</sub> in N<sub>2</sub>, and (c) in 1% CO and 1% O<sub>2</sub> in H<sub>2</sub> (PROX) at 383 and 523 K, respectively.

Table 2  
IR bands on ceria supported Pt in the 2200–1800  $\text{cm}^{-1}$  region

Name	Wavenumbers ( $\text{cm}^{-1}$ )		In N <sub>2</sub>		CO alone		CO + O <sub>2</sub>		PROX	
	Literature values	Our values	383 K	523 K	383 K	523 K	383 K	523 K	383 K	523 K
CO adsorbed on Ce <sup>4+</sup>	2177, 2156 [37], 2170–2127 [54]	2172–2154	–	–	+	+	+	+	low	+
CO adsorbed on Ce <sup>3+</sup>	2120–2127 [54]	2124	–	–	Always present, their distinction is difficult					
CO adsorbed on Pt(ox)	2122–2131 [35]	2121–2115	–	–						
CO adsorbed on metallic Pt with Pt(ox) neighbor	2091–2096 [34,35]	2095	–	–	+	low	+	low	low	low
CO linearly adsorbed on terraces	2080–2085 [14,15,34,35]	2083–2075	–	–	+	+	+	+	+	+
CO linearly adsorbed on step sites	2072–2065 [14,15,34,35]	2068–2041	–	–	+	+	+	+	+	+
CO on metal/support interface site	1960–1970 [33,49–52]	1960–1970	–	–	Always present, more at high <i>T</i>					
Bridged CO on Pt	1850 [14,33]	1877–1882	–	–	Only small amount at low <i>T</i>					

bonded CO species was resolved at 1880  $\text{cm}^{-1}$ . An additional weak  $\nu(\text{CO})$  band observed at ca. 2124  $\text{cm}^{-1}$  and a doublet encompassing broad bands at 2172 and 2157  $\text{cm}^{-1}$  have been ascribed to CO linearly adsorbed on reduced and unreduced ceria sites, respectively [37,54]. However, in our case these bands overlap with  $\nu(\text{CO})$  of the gaseous carbon monoxide, and only at ca. 2124  $\text{cm}^{-1}$  there is definitely a contribution from adsorbed CO, because the P branch (of gas-phase CO) is weaker than the R branch (above 2143  $\text{cm}^{-1}$ ).

Increasing temperature led to the following: (i) a decrease in intensity of the main band and of the shoulder at 2083  $\text{cm}^{-1}$  and a relative increase in intensity of the component at ca. 1970–1960  $\text{cm}^{-1}$ ; (ii) a shift of the main band to lower wavenumbers (from 2063 to 2051  $\text{cm}^{-1}$ ); (iii) a relative increase in the intensity of the  $\nu(\text{CO})$  band on Ce<sup>3+</sup> sites compared to that one on Ce<sup>4+</sup> sites; and (iv) a discernable feature at 2112  $\text{cm}^{-1}$ . The broad band at 2112  $\text{cm}^{-1}$  is due to CO linearly adsorbed both on Pt atoms interacting with oxygen (i.e., Pt atoms in a more unsaturated coordination state (Pt<sup>δ+</sup>) [34,35]) and on Ce<sup>3+</sup> sites, respectively.

In the presence of oxygen in the gas mixture (Fig. 4b), only moderate changes occurred compared with the CO alone case (Fig. 4a); most of the  $\nu(\text{CO})$  bands were slightly blue-shifted ( $\sim 5 \text{ cm}^{-1}$ ), with the intensity of the shoulder at 2095  $\text{cm}^{-1}$  relatively increased and that of the shoulder at 2083  $\text{cm}^{-1}$  decreased. These changes can be explained by slight oxidation (probably hindered reduction) of the Pt particles.

Under PROX conditions (Fig. 4c), a general shift to lower wavenumbers was observed, with the main band shifted from 2063 to 2054  $\text{cm}^{-1}$  and the shoulder positioned at 2075  $\text{cm}^{-1}$ . Increasing temperature in the presence of hydrogen resulted in a further shift of these  $\nu(\text{CO})$  bands to 2041 and 2068  $\text{cm}^{-1}$ , respectively, and a relative increase in intensity of the broad  $\nu(\text{CO})$  band at 1965  $\text{cm}^{-1}$  compared with that at  $T = 383 \text{ K}$ .

### 3.3.2. DRIFT spectra in the 1800–1000 $\text{cm}^{-1}$ region

The DRIFT spectra of the 1% Pt/CeO<sub>2</sub> sample under different conditions in the 1800–1000  $\text{cm}^{-1}$  region are shown in Fig. 5. In this region different carbonate, carboxylate and formate species gave several bands; their assignments are summa-

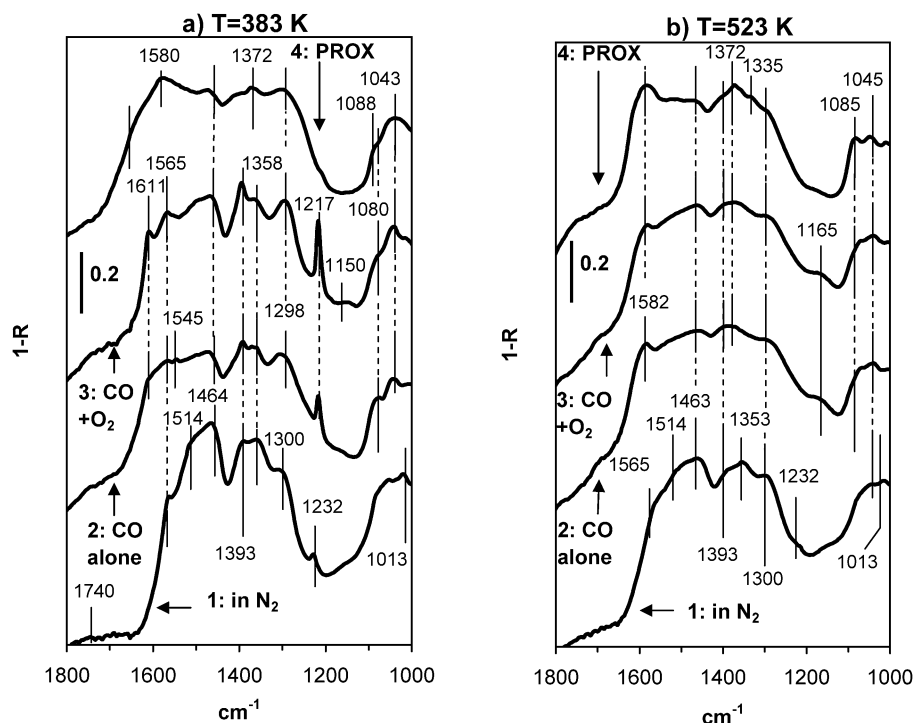


Fig. 5. DRIFT spectra in the 1800–1000  $\text{cm}^{-1}$  region (OCO vibrations) of 1% Pt/CeO<sub>2</sub> at (a)  $T = 383$  K and (b)  $T = 523$  K after activation, in the presence of 1% CO alone in N<sub>2</sub>, in 1% CO and 1% O<sub>2</sub> in N<sub>2</sub>, and in 1% CO and 1% O<sub>2</sub> in H<sub>2</sub> (PROX), respectively.

Table 3

IR bands on ceria supported Pt for carbonate and carboxylate species. Bands in *italic* are OH vibrations

Name	Formula	Wavenumbers ( $\text{cm}^{-1}$ )		In N <sub>2</sub>		CO alone		CO + O <sub>2</sub>		PROX	
		Literature values	Our values	383 K	523 K	383 K	523 K	383 K	523 K	383 K	523 K
Carbonate unidentate		1545, 1348, 1062 [36]	1464, 1358, 1085	+	+	+	+	+	+	+	+
Carbonate bidentate		1562, 1286, 1028 [36]	1565, 1298, 1014–1009	+	+	+	+	+	+	+	+
Carbonate polydentate	Polymer	1462, 1353, 1066 [33]	1463, 1353, 1050–1040	+	+	+	+	+	+	+	+
Bridged carbonate		1728, 1396, 1219, 1132 [36]	1740, 1393, 1232, 1145	+	-	+	-	+	-	-	-
Bicarbonate		3617, 1613, 1391, 1218, 1045 [33]	3619, 1611, 1393, 1217, 1043	-	-	+	-	+	-	-	-
Carboxylate		1560, 1510, 1310 [36]	1514, 1316	+	+?	?	+	?	+	-	-
Carboxylic acid		1670–1695, 1338–1310 [35,36]	3590, 1700–1600, 1335	-	-	+	+	+	+	+	+

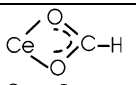
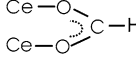
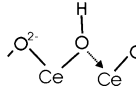
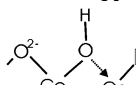
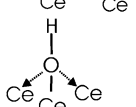
ized in Tables 3 and 4. The identification of carboxylic acids, bicarbonates and formate species were also based on their other characteristic O–H (Fig. 6) or C–H bands (Fig. 7), respectively.

Unidentate carbonate (strong bands at 1464 and 1358  $\text{cm}^{-1}$  and a weak band at 1080  $\text{cm}^{-1}$ ), bidentate carbonate (features at ca. 1565, 1300, and 1013  $\text{cm}^{-1}$ ), and traces of bicarbonate (medium bands at 1393 and 1232, a weak band at ca. 1050, and a shoulder at ca. 1611  $\text{cm}^{-1}$ ) and carboxylate (feature at ca. 1514 and a very weak band at 1316  $\text{cm}^{-1}$ ) species were present on the surface of the O<sub>2</sub> pretreated sample at  $T = 383$  K

in N<sub>2</sub> (Fig. 5a). Increasing temperature resulted in a decrease of the bicarbonate and slight increase of the bidentate carbonate species on the surface of the activated sample (Fig. 5b).

Exposure to 10 mbar of CO alone or in the presence of oxygen yielded bands that were grouped as follows: (i) strong bands at 1393 and 1217  $\text{cm}^{-1}$  and weak ones at 1611 and 1043  $\text{cm}^{-1}$ ; (ii) a strong broad band at 1298  $\text{cm}^{-1}$  and weak bands at 1565 and  $\sim 1010$   $\text{cm}^{-1}$ ; and (iii) a medium band at 1545  $\text{cm}^{-1}$  and weak bands at 1372 and 1360  $\text{cm}^{-1}$ . The first group of bands was assigned to bicarbonate species, which correlates

Table 4  
IR bands on ceria supported Pt for formate and –OH species. Bands in *italic* are OH or CH vibrations

Name	Formula	Wavenumbers (cm <sup>-1</sup> )		In N <sub>2</sub>		CO alone		CO + O <sub>2</sub>		PROX	
		Literature values	Our values	383 K	523 K	383 K	523 K	383 K	523 K	383 K	523 K
Bidentate formate		2945, 2852, 1558, 1369, 1329 [37] 2845, 1547, 1358 [55]	2936, 2848, 1545, 1372, 1360	–	–	+	+	–	+	+	+
Bridged formate		2933, 2852, 1575, 1358 [55], 2945, 1587, 1329 [37]	2950, 2844, 1582, 1372, 1330	–	–	+	+	–	+	+	+
Type I OH	Ce–OH	3710 [33,59] 3650 [59]	3708–3700	+	+	+	+	+	+	?	+
Type II-A OH		3680–3660 [33, 58]	3658–3667	+	+	+	+	+	+	?	+
Type II-B OH		3651 [33,58]	3619–3625	+?	+	+?	+	–	+	?	+
Type III OH		3500 [59], 3600 [33,58]	3517	+	+	+	+	+	+	+	+

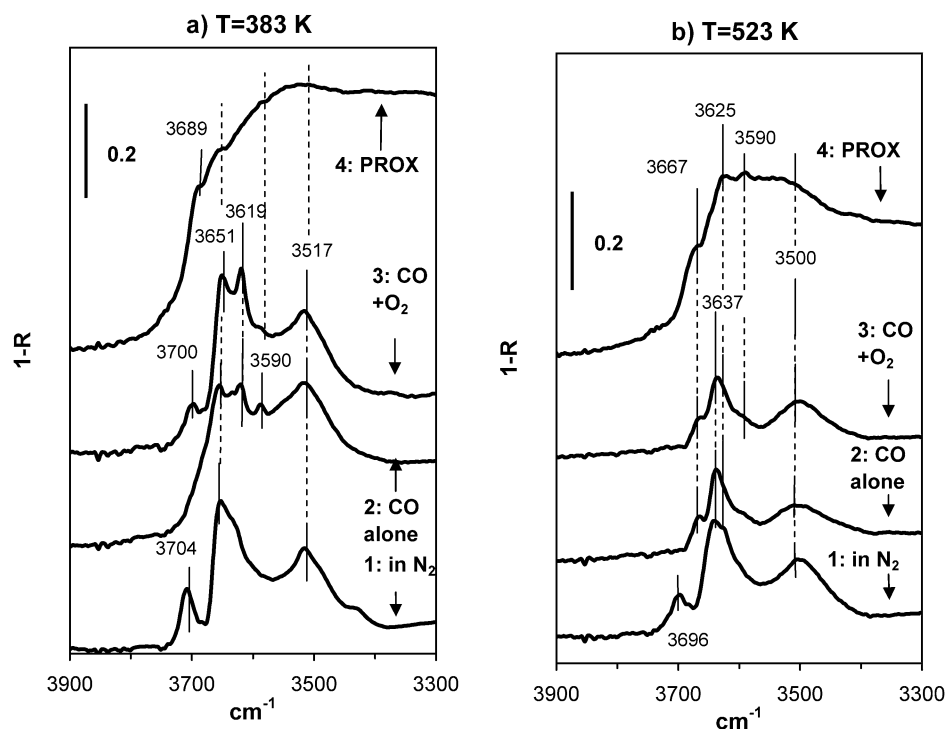


Fig. 6. DRIFT spectra in the 3900–3300 cm<sup>-1</sup> region (OH vibrations) of 1% Pt/CeO<sub>2</sub> at (a)  $T = 383$  K and (b)  $T = 523$  K after activation, in the presence of 1% CO alone in N<sub>2</sub>, in 1% CO and 1% O<sub>2</sub> in N<sub>2</sub>, and in 1% CO and 1% O<sub>2</sub> in H<sub>2</sub> (PROX), respectively.

well with the appearance of strong  $\nu(\text{OH})$  band at 3619 cm<sup>-1</sup> and concomitant decrease of another OH band (Fig. 6) observed on exposure of sample to CO or CO + O<sub>2</sub> gas mixtures. The second group of bands belongs to bidentate carbonate species. The relative intensities of the bands of different carbonate species were not affected by the presence of oxygen in the gas mixture, except for bands of bicarbonate, which were enhanced in CO + O<sub>2</sub> atmosphere. The third group of bands appearing only in the presence of CO alone, complemented by the appearance of  $\nu(\text{CH})$  bands (Fig. 7), belongs to bidentate formates formed

on partially reduced ceria through reaction between CO and surface hydroxyl groups [37].

Under PROX conditions, bicarbonate species observed in H<sub>2</sub>-free gas mixtures did not form (Fig. 5). The  $\nu(\text{OCO})$  bands of bidentate formate species became poorly resolved, with overall decreased intensities. At the same time, a strong broad feature developed at ca. 1582 cm<sup>-1</sup>, which may be attributed to the  $\nu_{\text{as}}(\text{OCO})$  band of bridged formate species [55]. The significant broadening above 1611 cm<sup>-1</sup> corresponds to surface water (see later). The  $\nu(\text{CO}_3)$  bands of bidentate and unidentate carbon-



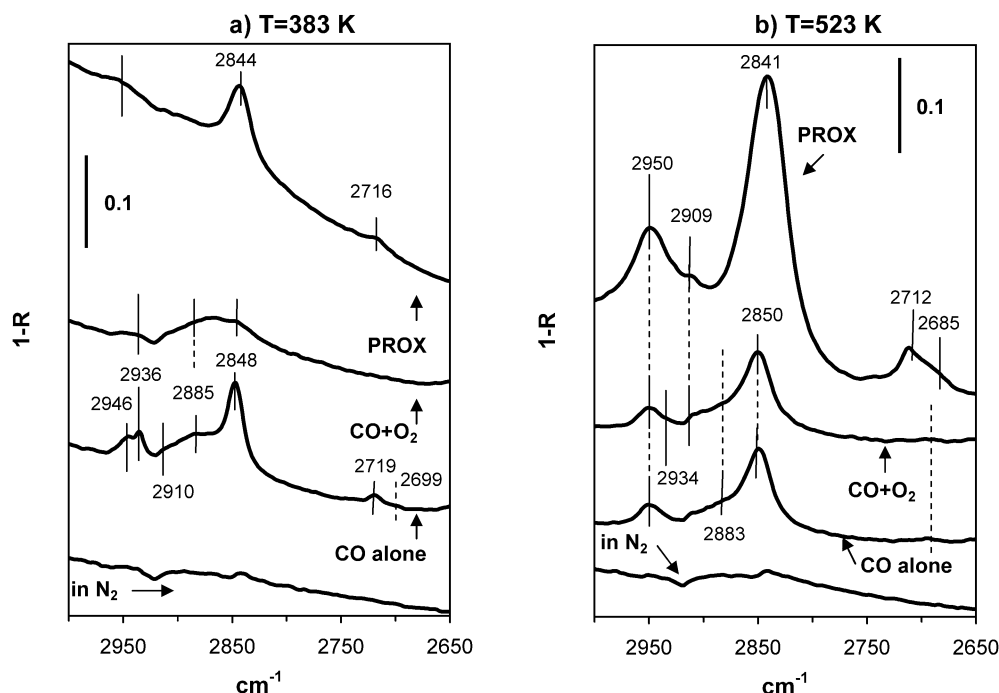


Fig. 7. DRIFT spectra in the 3000–2650 cm<sup>-1</sup> region (CH vibrations) of 1% Pt/CeO<sub>2</sub> at (a)  $T = 383$  K and (b)  $T = 523$  K after activation, in the presence of 1% CO alone in N<sub>2</sub>, in 1% CO and 1% O<sub>2</sub> in N<sub>2</sub>, and in 1% CO and 1% O<sub>2</sub> in H<sub>2</sub> (PROX), respectively.

ate species of similar intensities were present in the spectra in H<sub>2</sub>-rich atmosphere.

At  $T = 523$  K, the presence of CO alone and CO + O<sub>2</sub> gas mixtures gave a strong band at 1582 cm<sup>-1</sup> and weak bands at 1372, 1540, and 1360 cm<sup>-1</sup> (Fig. 5b), accompanied by the simultaneous appearance of a strong  $\nu$ (CH) band at 2850 cm<sup>-1</sup> (Fig. 7). These features indicate that bridged formate and probably traces of bidentate formate species are present on the surface. Under PROX conditions at  $T = 523$  K, bands belonging to bridged formate species (1582, 1372, and 1330 cm<sup>-1</sup>) were significantly higher than those at  $T = 383$  K in the presence of H<sub>2</sub> or at  $T = 523$  K in the absence of H<sub>2</sub>.

Ill-defined bands due to unidentate and/or polydentate [56] and bidentate carbonate species were also observed at  $T = 523$  K. Under PROX conditions, the poorly resolved bands at 1335, 1690, and 1510–1506 cm<sup>-1</sup> (Fig. 5) reflect the presence of protonated carboxylate species, carboxylic acid (–COOH), on the surface, as also indicated by the corresponding  $\nu$ (OH) 3590 cm<sup>-1</sup> (Fig. 6).

### 3.3.3. DRIFT spectra in the 3900–3300 cm<sup>-1</sup> region

Four OH groups were reproduced after oxidative activation on the 1% Pt/CeO<sub>2</sub> sample at  $T = 383$  K (Fig. 6a). They are denoted as type I, II, or III according to the number of cerium cations constituting the adsorption site [57]. The sharp peak at 3704 cm<sup>-1</sup> was assigned to mono-coordinated OH (type I); the band at 3651 cm<sup>-1</sup> with the shoulder at ca. 3625 cm<sup>-1</sup> was assigned to two types of bridging OH (types II-A and II-B); and a broad band centered at 3517 cm<sup>-1</sup> was assigned to triply bridging OH (III) species (Table 4) [58,59]. At  $T = 523$  K, a slight downshift of all  $\nu$ (OH) bands and a decrease in the number

of mono-coordinated (OH-I) and doubly bridging (OH-II) hydroxyl groups on the ceria surface was observed (Fig. 6b).

The presence of CO alone or O<sub>2</sub> + CO at  $T = 383$  K (Fig. 6a) resulted in the appearance of  $\nu$ (OH) bands at 3619 and 3590 cm<sup>-1</sup>, along with a decreased intensity of the  $\nu$ (OH-I) band at 3704 cm<sup>-1</sup>. The development of a strong band at 3619 cm<sup>-1</sup> and decaying of the band at 3704 cm<sup>-1</sup> were attributed to the formation of HCO<sub>3</sub><sup>-</sup> species through the reaction of CO with terminal (OH-I) hydroxyl groups. (Accordingly, bicarbonate vibrations were found in Fig. 5, as discussed earlier.) The other developed  $\nu$ (OH) band at 3590 cm<sup>-1</sup> may reflect the presence of carboxylic acid (–COOH) groups on the surface of the ceria support, because it correlates with the weak broad features observed under the same conditions at ca. 1690, 1510–1506, and 1330 cm<sup>-1</sup> (Fig. 5). Decreasing  $\nu$ (OH) bands can be correlated with the development of formate species, as described later.

The presence of oxygen had little effect on the position and relative intensities of the  $\nu$ (OH) bands, although the intensity of the band at 3704 cm<sup>-1</sup> was enhanced in the presence of oxygen compared with that in a CO-alone gas mixture (Fig. 6a). After CO adsorption at  $T = 523$  K, no distinct  $\nu$ (OH) band of bicarbonate species was resolved, whereas  $\nu$ (OH) stretching of all surface hydroxyl groups were downshifted ( $\sim 10$  cm<sup>-1</sup>) compared with that at  $T = 383$  K.

Under PROX conditions at  $T = 383$  K, isolated bands become convoluted into intense and broad absorption features, among which those centered at ca. 3689, 3658 (OH-IIA), and 3590 (carboxylic acid) could be somewhat resolved. Decreased resolution, a general broadening of stretching  $\nu$ (OH), and a strong increase in absorption toward lower wavenumbers indicate considerable H-bonding. A band at ca. 1640 cm<sup>-1</sup> and

the observation of H<sub>2</sub>O as a product are further evidence of the presence of significant amounts of water on the surface. H bonding with the Ce–OH groups suggests that the water is adsorbed predominantly on the support. Increasing temperature under PROX conditions decreased the intensity of features of adsorbed water and increased the intensity of the bands at 3625 cm<sup>-1</sup> (OH-IIB) and 3590 cm<sup>-1</sup>.

### 3.3.4. DRIFT spectra in the 3000–2650 cm<sup>-1</sup> region

The main bands in this vibration region can be assigned to bridged and bidentate formate species as follows (Fig. 7): 2848 cm<sup>-1</sup> as  $\nu(\text{CH})$ , 2936–2950 cm<sup>-1</sup> as a combination of  $\nu_{\text{as}}(\text{OCO})$  and the C–H in-plane vibration, and 2719 cm<sup>-1</sup> as overtone  $2\delta(\text{C–H})$ , which at around  $\delta(\text{C–H}) = 1360 \text{ cm}^{-1}$  is indeed hardly visible because of the strong carbonate vibrations (Fig. 5). The C–H vibrations of the two different formate species, bidentate and bridged, are quite similar; however, the difference in  $\nu_{\text{as}}(\text{OCO})$ — $\sim 1545 \text{ cm}^{-1}$  for bidentate and  $\sim 1582 \text{ cm}^{-1}$  for bridged (Table 4) [37,55]—makes their distinction possible. Consequently, the combination mode of  $\nu_{\text{as}}(\text{OCO})$  and the C–H in-plane vibration should also be higher for the bridged species than for the bidentate species [60].

After oxidative treatment of the Pt/CeO<sub>2</sub> sample, no bands were observed in the 3000–2600 cm<sup>-1</sup> region, whereas in CO stream, strong bands at 2936 and 2848 cm<sup>-1</sup> and weak features at ca. 2910, 2719, and ca. 2699 cm<sup>-1</sup> appeared (Fig. 7a). The main bands were assigned to surface formate species [37,61, 62], mainly to bidentate formate (see above). It was proposed that surface formate species on ceria were formed through the reaction of CO with terminal (OH-I) [55] and/or bridging (OH-II) [37,63] hydroxyl groups; these OH bands decreased accordingly, as discussed in the preceding section. The spectra under conditions of CO + O<sub>2</sub> exhibited no distinct bands in the 3000–2600 cm<sup>-1</sup> region. In the PROX gas mixture, at  $T = 383 \text{ K}$ , because of the strong “hydrogen-bonded OH–water structure,” the background increased as a function of wavenumbers, and thus the bands were poorly resolved. Nevertheless, a  $\nu(\text{CH})$  band at 2844 cm<sup>-1</sup> was observed, accompanied by weak broad features at ca. 2716 and 2952 cm<sup>-1</sup>. These bands might reflect the presence of both bidentate and bridged formate species on the surface [the latter probably being in excess, see corresponding  $\nu_{\text{as}}(\text{OCO})$  (Fig. 6)] or imply that the broad band at 2844 cm<sup>-1</sup> probably involves some contribution from  $\nu(\text{CH})$  vibrations, which are not associated with the formate species (hydrocarbonaceous residue).

At  $T = 523 \text{ K}$ , under conditions of CO alone and CO + O<sub>2</sub>, the position of the main  $\nu(\text{CH})$  band at 2848 cm<sup>-1</sup> was hardly affected. However, the ratio of bridged and bidentate formate species seemed to change; more bridged formate and less bidentate formate could be estimated than at low temperature, because of the relative increase in intensity of the band at 2950 cm<sup>-1</sup> and significant decrease in intensity of the band at 2936 cm<sup>-1</sup>, in accordance with the position of the corresponding  $\nu_{\text{as}}(\text{OCO})$  bands (see earlier). The presence of hydrogen in the gas mixture at elevated temperature resulted in a significant increase in intensity of the bands belonging to bridged formate species and the appearance of several weak bands that may be

assigned to the  $\nu(\text{CH})$  band of formyl species or may originate from other CH-containing species.

### 3.4. High-pressure XPS

The 5% Pt/CeO<sub>2</sub> sample was investigated in different gaseous environment using our novel high-pressure XPS setup [46,47]. The sample was first activated in 0.5 mbar O<sub>2</sub> at 573 K, then cooled in O<sub>2</sub>. At  $\sim 340 \text{ K}$ , oxygen was evacuated and replaced by hydrogen (0.48 mbar). As the ambient temperature was reached, first CO (0.032 mbar) and then O<sub>2</sub> (0.015 mbar) were added to the hydrogen. The surface state of the sample was investigated in these different environments. The catalytic activity observed during high-pressure XPS measurements is characterized in Table 1.

Fig. 8 depicts a part of the Ce 3d region in oxygen at 573 K, in hydrogen at 300 K, and in the PROX mixture at 358 K. As expected, the surface of ceria was more or less completely oxidized in oxygen, whereas hydrogen induced the formation of Ce<sup>3+</sup> species. The peaks V<sup>0</sup> at  $\sim 880.7 \text{ eV}$  and V' at  $\sim 885.5 \text{ eV}$  are characteristic for Ce<sup>3+</sup> species, whereas V ( $\sim 882.4 \text{ eV}$ ) and V'' ( $\sim 888.7 \text{ eV}$ ) correspond to oxidized ceria. (The same notation is used as established by Burroughs et al. [48] and popularly applied in other papers as well [38,39].) The use of 1035 eV synchrotron radiation ensures—due to the low KE electrons ( $\sim 140 \text{ eV}$  in this part of the spectrum)—that mainly the topmost few (two or three) Ce layers were probed. The reduction degree of ceria in hydrogen was estimated to be

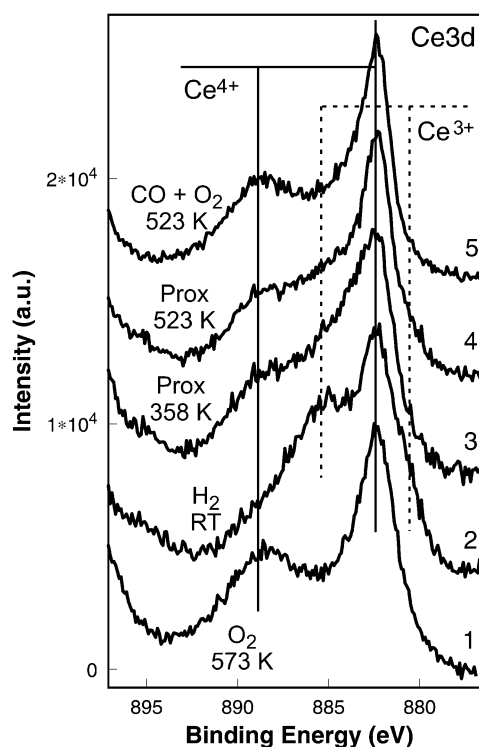


Fig. 8. Part of the Ce 3d region of the 5% Pt/CeO<sub>2</sub> at different conditions: 1, in 0.5 mbar O<sub>2</sub> at 573 K; 2, in 0.48 mbar H<sub>2</sub> at RT; 3, in  $\sim 0.5$  mbar PROX mixture at 358 K; 4, in  $\sim 0.5$  mbar PROX mixture at 523 K; 5, in a mixture of 0.032 mbar CO and 0.015 mbar O<sub>2</sub> (as hydrogen was switched off after 4). The measurements were carried out in sequence as indicated by the numbers.

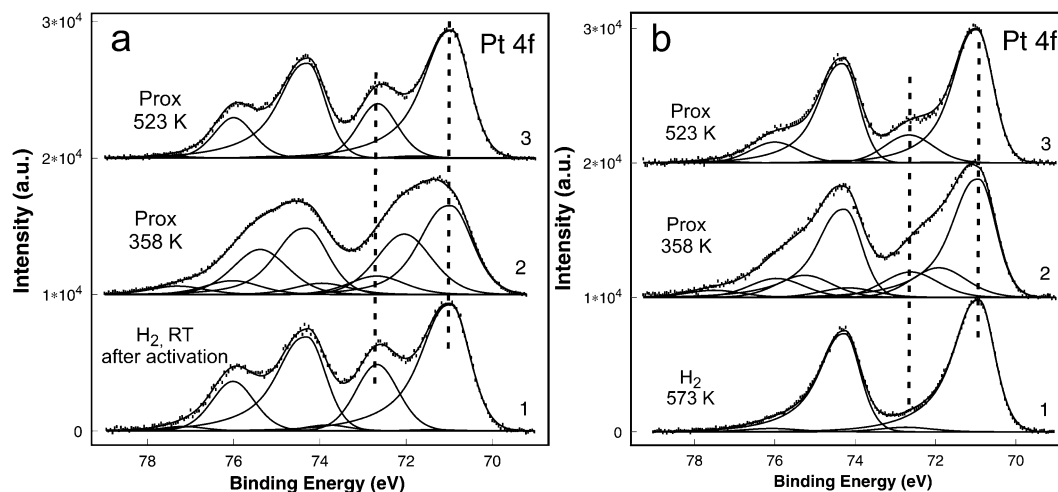


Fig. 9. (a) Pt 4f region of 5% Pt/CeO<sub>2</sub> at different conditions: **1**, in 0.48 mbar H<sub>2</sub> at RT (after O<sub>2</sub> activation at 573 K); **2**, in ~0.5 mbar PROX mixture at 358 K; **3**, in ~0.5 mbar PROX mixture at 523 K; (b) **1**, in 0.48 mbar H<sub>2</sub> at 573 K; **2**, in ~0.5 mbar PROX mixture at 358 K; **3**, in ~0.5 mbar PROX mixture at 523 K. The measurements were carried out in sequence as indicated by the numbers.

roughly 50%. Assuming that the reduction at low temperature affects just the top layer, this layer should be fully reduced to Ce<sup>3+</sup>. In the PROX mixture, the surface was clearly reoxidized, however. (Note that the gas mixture contained just 3% oxygen, whereas the other 97% had a reducing character.) This reoxidation was slightly more pronounced at 523 K, indicating that oxygen has a very strong sticking probability on ceria surfaces even at higher *T*. The ratio of the V to the V'' hybridization states changed in the PROX reaction mixture, although the surface was oxidized more or less similarly as in pure O<sub>2</sub>.

Fig. 9a shows the platinum 4f core level in hydrogen and in the reaction mixture at two different temperatures. In oxygen, charging of about 17 eV made the platinum peak (not shown) too broad to allow evaluation of its form. But introducing hydrogen at close to room temperature may induce hardly any changes in the valence state of platinum; thus we consider this spectrum representative for the oxygen-activated sample. The spectrum indicates two distinct components, one in the zero-valent state and the other with a BE shift of +1.6 eV. Identification of this second component is controversial according to the literature. Several studies found a Pt<sup>2+</sup> state (e.g., PtO) in a +1–1.8 eV distance relative to metallic Pt [64,65]; however, other studies [66,67] reported PtO in a +2.4–3 eV distance and PtO<sub>2</sub> at +3.6–4.5 eV [66,68]. Different surface–core level shift (SCLS) values were observed for adsorbed O<sub>2</sub> on Pt single crystals [67,69]. At this point, without arguing in favor of any of these possibilities, we call this component “Pt-oxidized1.” At 358 K under PROX conditions, the spectrum changed appreciably; this component was no longer resolved, and a shoulder at 72.0 eV appeared. The 7/2-to-5/2 splitting is still not well separated (intensity at ~73.5 eV); therefore, the Pt-oxidized1 component should not disappear completely. Moreover, a tail at around 77.2 eV is now clear, indicating a nonresolvable 7/2 component at ~73.9 eV. We call this “Pt-oxidized2.” According to the literature [69], SCLS of adsorbed CO gives BE shifts of ~+1.0 and +0.4 eV, identified as on-top and bridged bonded CO, respectively. Therefore, we may identify the 72.0 eV component as Pt with linearly bonded CO. On the other hand, the

fraction of this Pt species is too high to be explainable solely by surface Pt, because the spectra were taken with 460-eV photons, which are insufficiently surface-sensitive to account for such an intense component. Possible explanations could be that some special CO-induced compound-like platinum atoms give rise to this Pt 4f peak, or that the particles are extremely small and additional surface reconstruction occurs. Bridged CO cannot be resolved from our spectrum. On further heating of the sample to 523 K, the new peaks disappeared, and the spectrum closely resembled that measured after activation. The Pt-oxidized1 state decreased slightly in the reaction mixture.

In the second experiment, the sample after activation was reduced in hydrogen at 573 K and tested in the PROX reaction. The sample’s catalytic behavior was comparable to that of nonreduced sample, showing similar activity at low *T* and selectivity decay at 523 K. The corresponding spectra are shown in Fig. 9b. During the 573 K hydrogen treatment, platinum was totally reduced and could be fitted with the typical asymmetric function. In the PROX reaction mixture at low *T*, all the aforementioned components appeared, albeit at smaller relative intensities. This indicates that the Pt-oxidized1 species can be formed in the reaction mixture already at 358 K (or lower). Considering the high excess of reducing gases (H<sub>2</sub> and CO), the identification of this component as “bulk” PtO is not likely. It is more probable that, under less severe reducing conditions, the interface atoms are polarized by the negatively charged anions of the supporting ceria. If so, then the Pt particles should be very small (a few nm or even smaller).

Carbon 1s spectra of the activated sample in the reaction mixture at low and high temperatures are shown in Fig. 10. Because of variations in the form of the spectra, we used several components (actually, seven are shown) to adequately fit the measured curves. But unambiguous assignment is hardly possible, because many different species can have very similar BEs [70]. As a first approximation, we consider the lowest BE peak (284.2 eV) as graphene or graphite, the peaks around 286 eV as adsorbed CO in bridged (285.6 eV) and in linear (286.3 eV) coordination to Pt, and the other high-BE peaks

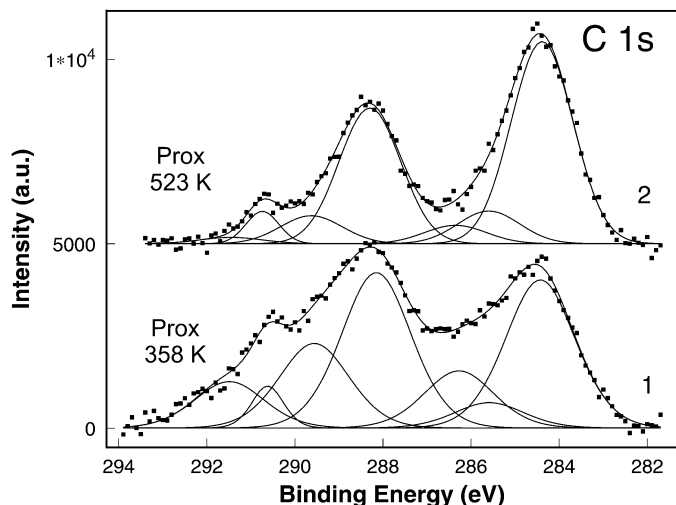
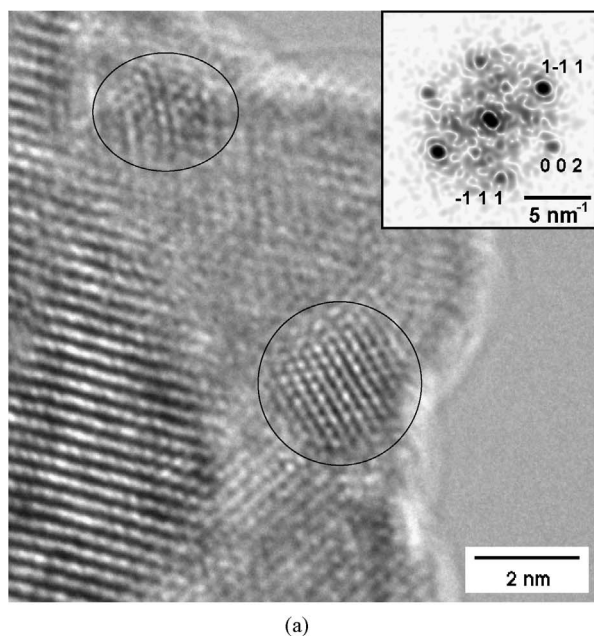


Fig. 10. C 1s region of 5% Pt/CeO<sub>2</sub> at different conditions: **1**, in ~0.5 mbar PROX mixture at 358 K; **2**, in ~0.5 mbar PROX mixture at 523 K.

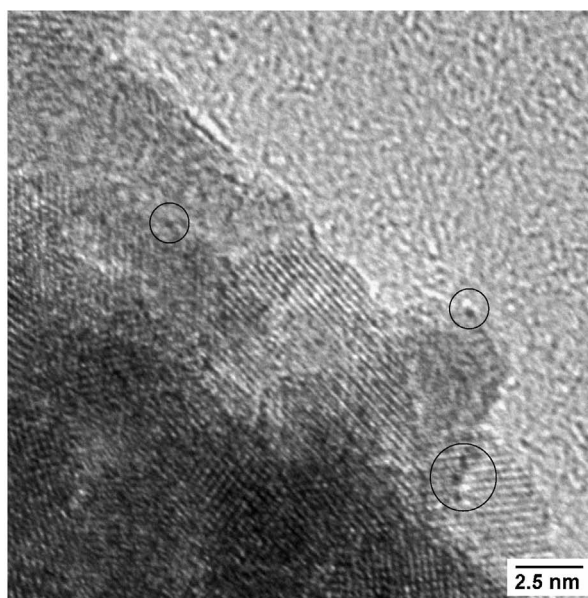
(except that of 290.6 eV, which is gas-phase CO) as different oxidized carbon on Pt, but mainly on the ceria surface. Because only a negligible amount of bridged CO (i.e., bonded between two Pt atoms) was detected by DRIFTS, the species at 285.6 may belong to CO bonded to the Pt–ceria interface (CO band at ~1960 cm<sup>-1</sup>). But this interface CO can be considered bridged adsorbed CO as well, considering that C is coordinating to Pt and O is interacting with a coordinatively unsaturated (cus) Ce<sup>n+</sup> site.

### 3.5. High-resolution transmission electron microscopy

High-resolution transmission electron microscopy (HRTEM) measurements were performed on the activated 5% Pt/CeO<sub>2</sub> to



(a)



(b)

Fig. 11. (a) High-resolution TEM image of 5% Pt/CeO<sub>2</sub> after activation in oxygen at 573 K. The inset shows the power spectrum of the platinum particle situated in the middle of the TEM image. (b) Other section of the sample showing very small dark spots (indicated by circles) that might correspond to Pt clusters in the size of 5–6 Å.

characterize the microstructure of the sample and to try to identify oxidized Pt (see above). The ceria particles (8–10 nm) were strongly stacked together despite the careful sample preparation, allowing no phase identification in most of the area of the specimen. Furthermore, depicting platinum particles was widely hindered by the strong contrast of the ceria lattice. Therefore, very few Pt particles could be found. A selected image is shown in Fig. 11a, in which accidentally two Pt particles can be seen. The particle about 2 × 3 nm in size is [110] oriented, as can be deduced from its power spectrum (see the inset). [The power spectrum is the square of the modulus of the Fourier transform of the two-dimensional image (or a chosen part of the image) and represents the (computer-generated) diffraction pattern of the image.] The contrast of the particle was slightly enhanced by filtering the corresponding spots (inverse lattice fringes) of the power spectrum, back-transforming, and adding it to the original image. Fig. 11b shows another part of the sample with unidentified dark spots on the surface of ceria. These spots did not behave like the dark and light spots in the carbon foil (*flickering*), and thus they do not belong to the foil, but may be very small (5–6 Å) Pt clusters. If so, then they should be partially oxidized through the relatively strong interaction with ceria. Oxidized “bulk” platinum could not be found in any form on the images, however. Therefore, we identify the 72.6 eV Pt 4f component as small Pt clusters (or interface Pt atoms) strongly interacting with ceria. Most of the ceria particles were in the form of CeO<sub>2</sub> (fluorite structure) with [110], [111], and [001] orientation. In some cases a small lattice expansion and a stronger angular distortion could be calculated mainly because of some defective structure. In addition, EDX measurements were carried out to roughly characterize the bulk Pt content of the sample. Using an area of 300 nm in diameter, the calculated Pt content was ~4 wt%. Using several small

(13 nm) regions, calculations give a minimum value of 4 wt% and a maximum value of 5.3 wt%; thus, platinum should be distributed quite homogeneously in the sample.

HRTEM after PROX reaction found a markedly higher number of reduced ceria particles with a more pronounced reduction degree. Careful analysis of the ceria particles revealed an oxygen-deficient structure ( $\text{CeO}_{1.695}$ ) in which the vacancies ordered and formed a supercell with a lattice constant more than twice that of  $\text{CeO}_2$ . For further details, see Part II.

#### 4. Discussion

Interaction of *CO alone* with the preoxidized catalyst can be seen in DRIFT spectra mainly as CO bonded to the metallic particles (Fig. 4). This adsorbed CO can then react with spilled-over oxygen to form gas-phase  $\text{CO}_2$  (observed at those times in the gas-phase spectra during DRIFTS experiments, but not shown here) [24–26,44]. The TDS measurement of adsorbed CO (Fig. 2) confirms this model. CO adsorbed on ceria sites and/or spilled over from the metal to the support was present only in a low proportion (Fig. 4), whereas a pronounced increase in the carboxyl region at  $1800\text{--}1000\text{ cm}^{-1}$  was observed (Fig. 5). Thus, CO on support sites must have oxidized rapidly to form different types of carbonate species [44]. The pronounced  $\text{CO}_2$  desorption on CO adsorption in the TDS spectra (Fig. 2) also supports this idea. At the same time, the interaction of CO species with the support OH groups ( $3704\text{ cm}^{-1}$ ) results in the formation of formate and bicarbonate species, as clearly shown in Figs. 5–7.

In the case of CO oxidation with oxygen, mainly the same changes were observed in the DRIFT spectra as in experiments with CO alone. The only difference was that the  $\nu(\text{CO})$  bands at  $2060\text{--}2100\text{ cm}^{-1}$  were slightly blue-shifted and the bands in the C–H region were less pronounced when oxygen was present; they even disappeared at  $T = 383\text{ K}$ . Thus, the presence of oxygen hardly affected CO adsorption and suppressed the formation of C–H bands.

The first observation indicates that the reaction mechanism (surface species) must have been the same in the experiments with CO alone and with CO +  $\text{O}_2$ . The role of oxygen was limited to reoxidation of support sites, because the Pt particles were almost totally covered with CO, as postulated earlier [18,24–26]. It correlates well with the observed strong affinity of partly reduced ceria surface toward gas-phase oxygen; it can be reoxidized even at low temperatures ( $T = 358\text{ K}$ ) in the presence of the PROX mixture, 3%  $\text{O}_2$  (see Fig. 8). Accordingly, the participation of oxygen from the ceria support in CO oxidation was proved earlier both from the observation of zero-order oxygen pressure dependence and from oxygen-exchange measurements between  $\text{C}^{16}\text{O}$ - and  $^{18}\text{O}$ -predosed catalysts [21].

Disproportionation of carbon monoxide  $2\text{CO} \rightarrow \text{C} + \text{CO}_2$  is another reported reaction pathway for OSC measurement on Pt/ $\text{CeO}_2$  at high temperatures [44]. The spillover and interaction of this carbon species with OH groups can also result in the formation of bands in the region of CH vibrations. Nevertheless, the reaction mechanism of CO disproportionation is not clarified. In fact, this process can take place via dissociation of CO and then reaction of the left-over oxygen with another adsorbed CO molecule.

The suppression of C–H bond formation results from excess oxygen present in the gas phase reoxidizing these species to carbonates or to  $\text{CO}_2$ . However, at high temperature, concomitantly with the evolution of these bands, the formation of gas-phase  $\text{CO}_2$  is suppressed (Fig. 12). The additional increase in the C–H region is attributed not to formates, but rather to methylidyne or partly hydrogenated graphitic species (Fig. 10) formed after CO dissociation.

In the presence of the PROX reaction mixture, a completely different picture is observed in the OH region of DRIFT spectra (Fig. 6). Poorly resolved overlapping curves were observed at  $T = 383\text{ K}$ , indicating a strong hydrogen-bonded system on the surface. Accordingly, XPS of the O 1s region also indicated a pronounced amount of adsorbed water on the ceria surface at low temperatures (see Part II, in comparison with Pd/ $\text{CeO}_2$ ). At

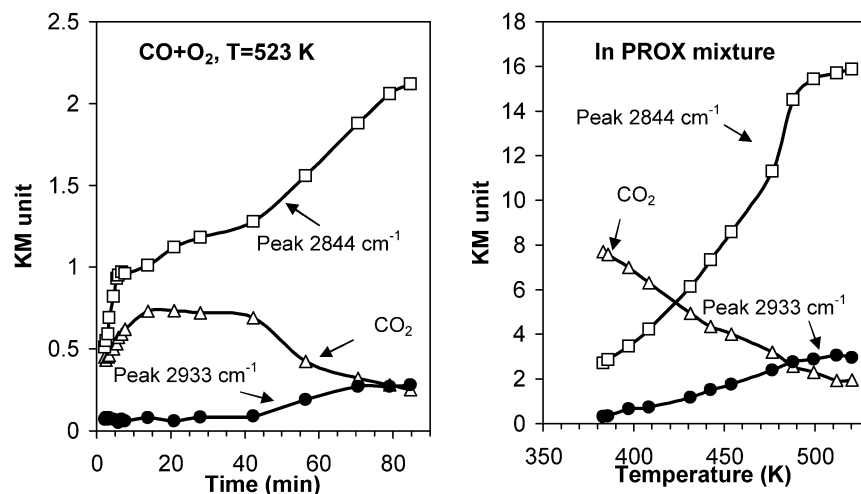


Fig. 12. Correlation of integrated intensities of surface C–H bands and gas-phase  $\text{CO}_2$  band. Both of them originate from in situ DRIFTS data and are expressed in Kubelka–Munk (KM) units.

the same time, ceria was reduced only slightly at low temperatures (Fig. 8).

Before the reaction mechanism for the PROX reaction is described, it must be emphasized that Pt itself is active both in hydrogen and CO oxidation, and an obvious reaction route is that products of these reactions, CO<sub>2</sub> and H<sub>2</sub>O, desorb from Pt. The selectivity is determined only by the competitive adsorption of CO, H<sub>2</sub>, and O<sub>2</sub>, as has been clearly shown for the Pt/Al<sub>2</sub>O<sub>3</sub> system [11,13]. In this case, hydrogen adsorption on Pt (and hence the possibility toward nonselective oxidation), is strongly suppressed by the high (but not total) CO coverage, even in excess H<sub>2</sub>. Nevertheless, Pt/CeO<sub>2</sub> behaves differently than Pt/Al<sub>2</sub>O<sub>3</sub> in the PROX reaction [13], as emphasized earlier.

Our results show that accumulation of both CO<sub>2</sub> (in the form of carbonates and formates) and H<sub>2</sub>O (in “hydrogen-bonded OH–water structure”) is possible on the ceria support, especially at lower temperatures. These structures can be formed either by spillover of reaction products (CO<sub>2</sub> and H<sub>2</sub>O) or, more likely, by spillover of hydrogen or CO to the support. The possibility of direct adsorption (e.g., H<sub>2</sub> [71]) on the support also cannot be neglected. Among all of these possibilities, hydrogen spillover is the most likely. The hydrogen on the support reacts rapidly with oxidized ceria to form OH groups on the surface, whereas ceria is reduced to Ce<sup>3+</sup> and adsorbed water accumulates on the ceria surface. This water then reacts with carbonate and carboxylate groups, resulting in hydroxylation of the surface (see the relatively high amount of carboxylic acid in the PROX reaction, as revealed by DRIFTS). The reduced Ce<sup>3+</sup> centers on the surface seem to be reoxidized; however, HRTEM indicates that these reduced defect sites formally move into the bulk of ceria, forming an oxygen-deficient supercell during the reaction. The presence of adsorbed water seems to suppress hydrogen oxidation while CO oxidation still occurs, as the metallic particles are covered by CO, and most probably because oxygen spillover to the metallic site is not hindered by this hydrogen-bonded structure. The promoting effect of surface water on CO oxidation over Pt catalysts was postulated recently on microkinetic modeling [72]. The possibility of a direct contribution of water in a low-temperature water–gas shift (LTWGS)-type reaction has also been proposed [72]. In this way, surface water (and/or OH groups) would react at the perimeter of Pt particles with linearly bonded CO molecules [72] or with surface formate [63,73] or carboxyl species [72], which are thought to be intermediates in a LTWGS reaction producing CO<sub>2</sub> and H<sub>2</sub>. Each of these possibilities would result in relatively high selectivity toward CO oxidation in the PROX reaction at low temperature.

Increasing the temperature in the PROX reaction leads to the following: (i) decreased selectivity toward CO oxidation (Figs. 1 and 12); (ii) further oxidation of the ceria surface (Fig. 8); (iii) decreased linearly adsorbed CO species seen both in XPS (Fig. 10) and DRIFTS (Fig. 4); (iv) increase of the band around 1965 cm<sup>-1</sup> (Fig. 4); (v) increased intensity of C–H vibrations in the DRIFT spectra (Fig. 7); (vi) increased amount of graphite-like species in the C 1s XP spectra (Fig. 10); and (vii) decreased surface OH–water H-bonded structure (Fig. 6).

The interaction of CO at the metal–support interface with the Ce cation gives rise to a strong enhancement of the band at ~1965 cm<sup>-1</sup> as most of the water desorbs from ceria, in good agreement with the findings of Kappers et al. [53]. This “bridged-like” interface species correlates with the enhanced intensity in the C 1s region identified as bridged CO. Its pronounced appearance is accompanied by increased C–H vibration in DRIFT spectra and, accordingly, in the XPS C 1s region. We suggest that this band at 1960–1970 cm<sup>-1</sup> is a possible precursor for CO dissociation on the boundary site, and thus the precursor for methylidyne or hydrogenated graphitic species. At the same time, formate species became more pronounced. If CO does not dissociate at the interface but rather hops to the ceria, then surface formates can be formed in the reaction with OH groups. But in the absence of surface water, they accumulate near the Pt particles and represent a “dead end” for the reaction. The formation of all of the aforementioned (C–H) species shows an apparent negative correlation with CO<sub>2</sub> production (Fig. 12); thus the catalyst is deactivating.

To sum up, the most feasible mechanism for CO oxidation in PROX mixture is as follows. At the beginning, a significant amount of water accumulates on the ceria via spillover of adsorbed hydrogen atoms from the platinum. This water reacts in a LTWGS reaction with *linearly* bonded CO at the Pt–ceria interface, forming CO<sub>2</sub> and hydrogen. Hydrogen instead of desorption regenerates surface water by reacting with oxygen. At high *T*, the hydrogen-bonded structure decomposes and water desorbs. As a result, CO can bind in *bridged-like* manner at the interface, giving rise to dissociation and/or formate formation. Thereafter, the empty interface site can be quickly refilled by a new CO molecule, continuing this side reaction. Although surface formates as intermediates in PROX cannot be completely excluded, they seem to represent a rather dead end for the reaction. The key feature appears to be the *linearly* bonded CO at the Pt–ceria interface in a close interaction with surface water.

## 5. Conclusions and summary

The preferential oxidation of CO in the presence of excess hydrogen (PROX) on Pt/CeO<sub>2</sub> catalysts was examined by different spectroscopic techniques (DRIFTS and XPS) in combination with catalytic measurements in desired in situ apparatuses. Characterization of the sample by TDS and TEM gave corresponding results. The first major conclusion of this paper is that the results of these techniques, especially in situ DRIFTS (surface species) and high-pressure XPS (oxidation states under reaction conditions), complement one another perfectly. The catalytic data of the PROX reaction measured in the two in situ spectroscopic systems showed trends identical to those determined in the atmospheric catalytic reactor.

The surface species determined by DRIFTS in the presence of CO alone and a CO + O<sub>2</sub> mixture were very similar. Thus CO oxidation would occur similarly in the presence and the absence of oxygen, supporting the mechanism of CO oxidation proposed earlier for ceria-supported noble metal catalysts. The role of gas-phase oxygen is limited to the regeneration of reduced ceria sites; however, in the presence of hydrogen, the

carbonate and formate species found by DRIFTS during the PROX reaction strongly indicate that this reaction differs from CO oxidation.

DRIFTS found no resolved OH bands in the PROX reaction mixture, indicating a significant amount of adsorbed water on the ceria surface in a hydrogen-bonded structure. Its presence seems to suppress hydrogen oxidation while CO oxidation still occurs, as the metallic particles are covered by CO (DRIFTS). On the other hand, no direct correlation between CO coverage and CO<sub>2</sub> formation was found. The direct contribution of surface water in a LTWGS reaction, causing apparently high selectivity toward CO oxidation, was established. Increasing temperature leads to slightly decreased CO coverage on metal particles, desorption of surface water, and increase of formate species. This latter two effects decrease the selectivity toward CO oxidation as a function of temperature.

Earlier investigations of the PROX reaction aimed at suppressing hydrogen adsorption on the catalyst (usually metal) surface while keeping CO adsorption and oxygen activation (usually on different sites) possible. But our results point to the beneficial effect of surface water, which suppresses further hydrogen oxidation and can directly participate in the water-gas shift reaction. Another possible way to prepare a highly selective PROX catalyst is to suppress water desorption (and not water formation) and promote a LTWGS reaction. Further investigation into more realistic (water- and CO<sub>2</sub>-containing) reaction mixtures is planned.

## Acknowledgments

Financial support was provided by the Hungarian National Science Foundation (grant OTKA F046216), National R&D Program (NKFP 3A058-04), the Athena Consortium, and the Hungarian Academy of Sciences (a Bolyai grant to A.W.). The authors thank the BESSY staff for providing technical assistance during the in situ XPS measurements.

## References

- [1] A.J. Appleby, F.R. Foulkes, *Fuel Cell Handbook*, Van Nostrand Reinhold, New York, 1989.
- [2] J.N. Armor, *Appl. Catal.* 176 (1999) 159.
- [3] F. Aupretre, C. Descorme, D. Duprez, *Catal. Commun.* 3 (2002) 263.
- [4] C.D. Dudfield, R. Chen, P.L. Adock, *Int. J. Hydrogen Energy* 26 (2001) 763.
- [5] S.H. Lee, J. Han, K.-Y. Lee, *J. Power Sources* 109 (2002) 394.
- [6] G. Avgouropoulos, T. Ioannides, Ch. Papadopoulou, J. Batita, S. Hococevar, H.K. Martalis, *Catal. Today* 75 (2002) 157.
- [7] G.K. Bethke, H.H. Kung, *Appl. Catal.* 194–195 (2000) 43.
- [8] M.J. Kahlich, H. Gasteiger, R.J. Behm, *J. Catal.* 182 (1999) 430.
- [9] M.M. Schubert, M.J. Kahlich, H.A. Gasteiger, R.J. Behm, *J. Power Sources* 84 (1999) 175.
- [10] S.H. Oh, R.M. Sinkevitch, *J. Catal.* 142 (1993) 254.
- [11] M.J. Kahlich, H.A. Gasteiger, R.J. Behm, *J. Catal.* 171 (1997) 93.
- [12] S. Özkara, A.E. Aksoylu, *Appl. Catal. A* 251 (2003) 75.
- [13] A. Wootsch, C. Descorme, D. Duprez, *J. Catal.* 225 (2004) 259.
- [14] Y.-F. Han, M.J. Kahlich, M. Kinne, R.J. Behm, *Phys. Chem. Chem. Phys.* 4 (2002) 389.
- [15] M.M. Schubert, M.J. Kahlich, G. Feldmeyer, M. Hüttner, S. Hackensberg, H.A. Gasteiger, R.J. Behm, *Phys. Chem. Chem. Phys.* 3 (2001) 1123.
- [16] M. Haruta, *Catal. Today* 36 (1997) 153.
- [17] X. Liu, O. Korotkikh, R. Farrauto, *Appl. Catal. A* 226 (2002) 293.
- [18] A. Trovarelli, *Catal. Rev. Sci. Eng.* 38 (1996) 439.
- [19] Y.Y. Yung-Fang, *J. Catal.* 87 (1984) 162.
- [20] S. Johansson, L. Österlund, B. Kasemo, *J. Catal.* 201 (2001) 275.
- [21] R. Taha, D. Martin, S. Kacimi, D. Duprez, *Catal. Today* 29 (1996) 89.
- [22] T. Bunluesin, H. Cordatos, R.J. Gorte, *J. Catal.* 157 (1995) 222.
- [23] E. Bekyarova, P. Fornasiero, J. Kaspar, M. Graziani, *Catal. Today* 45 (1998) 179.
- [24] H.C. Yao, Y.F. Yu-Yao, *J. Catal.* 86 (1984) 254.
- [25] S. Bedrane, C. Descorme, D. Duprez, *Catal. Today* 73 (2002) 233.
- [26] S. Bedrane, C. Descorme, D. Duprez, *Catal. Today* 75 (2002) 401.
- [27] S. Bernal, J.J. Calvino, G.A. Cifredo, J.M. Rodríguez-Izquierdo, V. Perrichon, A. Laachir, *J. Catal.* 137 (1992) 1.
- [28] S. Salasc, V. Perrichon, M. Primet, M. Chevrier, N. Mouaddib-Moral, *J. Catal.* 189 (2000) 401.
- [29] S. Bernal, J.J. Calvino, M.A. Cauqui, J.M. Gatica, C. Larese, J.A. Pérez Omil, J.M. Pintado, *Catal. Today* 50 (1999) 175.
- [30] W.J. Shen, Y. Ichihashi, H. Ando, Y. Matsumura, M. Okumura, M. Haruta, *Appl. Catal. A* 217 (2001) 231.
- [31] G. Rupprechter, J.J. Calvino, C. López-Cartez, M. Fuchs, J.M. Gatica, J.A. Pérez-Omil, K. Hayek, S. Bernal, *Stud. Surf. Sci. Catal.* 130 (2000) 2021.
- [32] A. Holmgren, B. Andersson, D. Duprez, *Appl. Catal. B* 22 (1999) 215.
- [33] C. Binet, M. Daturi, J.-C. Lavalley, *Catal. Today* 50 (1999) 207.
- [34] D.W. Daniel, *J. Phys. Chem.* 92 (1988) 3891.
- [35] T. Jin, Y. Zhou, G.J. Mains, J.M. White, *J. Phys. Chem.* 91 (1987) 5931.
- [36] C. Li, T. Arai, K. Domen, K. Maruya, T. Onishi, *J. Chem. Soc., Faraday Trans.* 85 (1989) 929.
- [37] C. Li, Y. Sakata, T. Arai, K. Domen, K. Maruya, T. Onishi, *J. Chem. Soc., Faraday Trans.* 85 (1989) 1451.
- [38] A. Pfau, K.D. Schierbaum, *Surf. Sci.* 321 (1994) 71.
- [39] A.Q. Wang, P. Punchnaipetch, R.M. Wallace, T.D. Golden, *J. Vac. Sci. Technol. B* 21 (2003) 1169.
- [40] M.A. Henderson, C.L. Perkins, M.H. Engelhard, S. Thevuthasan, C.H.F. Peden, *Surf. Sci.* 526 (2003) 1.
- [41] Y. Madier, C. Descorme, A.M. Le Govic, D. Duprez, *J. Phys. Chem. B* 103 (1999) 10999.
- [42] D. Teschner, A. Wootsch, K. Matusek, T. Röder, Z. Paál, *Solid State Ionics* 141 (2001) 709.
- [43] S. Kacimi, J. Barbier Jr., R. Taha, D. Duprez, *Catal. Lett.* 22 (1993) 343.
- [44] A. Holmgren, B. Andersson, *J. Catal.* 178 (1998) 14.
- [45] D.F. Ogletree, H. Bluhm, G. Lebedev, C. Fadley, Z. Hussain, M. Salmeron, *Rev. Sci. Instrum.* 73 (2002) 3872.
- [46] D. Teschner, A. Pestryakov, E. Kleimenov, M. Hävecker, H. Bluhm, H. Sauer, A. Knop-Gericke, R. Schlögl, *J. Catal.* 230 (2005) 186.
- [47] D. Teschner, A. Pestryakov, E. Kleimenov, M. Hävecker, H. Bluhm, H. Sauer, A. Knop-Gericke, R. Schlögl, *J. Catal.* 230 (2005) 195.
- [48] P. Burroughs, A. Hamnett, A.F. Orchard, G. Thornton, *J. Chem. Soc. Dalton Trans.* 17 (1976) 1686.
- [49] D. Ferri, T. Bürgi, A. Baiker, *Phys. Chem. Chem. Phys.* 4 (2002) 2667.
- [50] R. Barth, R. Pitchai, R.L. Anderson, X.E. Verykios, *J. Catal.* 115 (1989) 61.
- [51] J. Silvestre-Albero, A. Sepulveda-Escribano, F. Rodríguez-Reinoso, J.A. Anderson, *Phys. Chem. Chem. Phys.* 5 (2003) 208.
- [52] P. Hollins, *Surf. Sci. Rep.* 16 (1992) 51.
- [53] M.J. Kappers, J.T. Miller, D.C. Koningsberger, *J. Phys. Chem.* 100 (1996) 3227.
- [54] F. Bonzon-Verduraz, A. Bensalem, *J. Chem. Soc., Faraday Trans. I* 90 (1994) 653.
- [55] T. Shido, Y. Iwasawa, *J. Catal.* 136 (1992) 493.
- [56] C. Binet, M. Daturi, J.C. Lavalley, *Catal. Today* 50 (1999) 207.
- [57] A. Tsyganenko, V. Filimonov, *J. Mol. Struct.* 19 (1973) 579.
- [58] A. Badri, C. Binet, J.C. Lavalley, *J. Chem. Soc., Faraday Trans.* 92 (1996) 4669.
- [59] A. Laachir, V. Perrichon, A. Badri, J. Lamotte, E. Chaterine, J.C. Lavalley, J. El Fallah, L. Hilaire, F. Le Normand, E. Quemere, G.N. Sauvion, O. Touret, *J. Chem. Soc., Faraday Trans.* 87 (1991) 1601.
- [60] K. Nakamoto, *IR and Raman Spectra of Inorganic and Coordination Compounds*, Wiley-Interscience, New York, 1987.

- [61] G. Busca, J. Lamotte, J.C. Lavalley, V. Lorinzelli, *J. Am. Chem. Soc.* 109 (1987) 5197.
- [62] C. Li, K. Domen, K. Maruya, T. Onishi, *J. Catal.* 125 (1990) 445.
- [63] G. Jacobs, U.M. Graham, E. Chenu, P.M. Patterson, A. Dozier, B.H. Davis, *J. Catal.* 229 (2005) 499.
- [64] M.-C. Jung, H.-D. Kim, M. Han, W. Jo, D.C. Kim, *Jpn. J. Appl. Phys.* 38 (1999) 4872.
- [65] J.S. Hammond, N. Winograd, *J. Electrochem. Electroanal. Chem.* 78 (1977) 55.
- [66] K.S. Kim, N. Winograd, R.E. Davis, *J. Am. Chem. Soc.* 93 (1971) 6296.
- [67] C.R. Parkinson, M. Walker, C.F. McConville, *Surf. Sci.* 545 (2003) 19.
- [68] J.L.G. Fierro, J.M. Palacios, F. Tomas, *Surf. Interface Anal.* 13 (1988) 25.
- [69] K. Dücker, K.C. Price, H.P. Bonzel, V. Chab, K. Horn, *Phys. Rev. B* 36 (1987) 6292.
- [70] N.M. Rodriguez, P.E. Anderson, A. Wootsch, U. Wild, R. Schlögl, Z. Paál, *J. Catal.* 197 (2001) 365.
- [71] S. Bernal, J.J. Calvino, G.A. Cifredo, J.M. Gatica, J.A.P. Omil, J.M. Pintado, *J. Chem. Soc., Faraday Trans.* 89 (1993) 3499.
- [72] A.B. Mhadeshwar, D.G. Vlachos, *J. Phys. Chem. B* 108 (2004) 15246.
- [73] G. Jacobs, P.A. Patterson, U.M. Graham, D.E. Sparks, B.H. Davis, *Appl. Catal. A* 269 (2004) 63.